Influence of the Preparation Method on the Surface Characteristics and Activity of Boron-Nitride-Supported Noble Metal Catalysts

Georgeta Postole,[†,||] Antonella Gervasini,[‡] Claude Guimon,[§] Aline Auroux,*[,†] and Bernard Bonnetot[⊥]

Institut de Recherches sur la Catalyse, Centre National de la Recherche Scientifique, 2 Av. A. Einstein, 69626 Villeurbanne Cedex, France, Dipartimento di Chimica Fisica ed Elettrochimica and Centro di Eccellenza, Centro Interdisciplinare Materiali e Interfacce Nanostrutturati, Università di Milano, via Golgi 19, I-20133 Milano, Italy, LPCM, Université de Pau, 2 Av. P. Angot, 64053 Pau Cedex 09, France, "Ilie Murgulescu" Institute of Physical Chemistry of the Romanian Academy, Spl. Independentei 202, 060041 Bucharest, Romania, and Laboratoire Multimatériaux et Interfaces, CNRS UMR 5615, Université Claude Bernard Lyon 1, 69622 Villeurbanne Cedex, France

Received: January 10, 2006; In Final Form: April 26, 2006

In this article, we report how variations in the preparation method of boron-nitride-supported noble metal catalysts may influence the surface characteristics of the active phase and consequently the potential applications as catalysts for oxidation reactions. The deposition and the dispersion of the active phase are strongly influenced by the preparation process and in particular by the protic or aprotic solvent used as the dispersing phase; in this study, benzene, glyme, water, tetrahydrofuran, diglyme, 2-propanol, and glycol have been investigated. Characterization techniques, such as Brunauer−Emmett−Teller, X-ray diffraction, transmission electron microscopy, Fourier transform infrared spectroscopy, and thermogravimetric analysis, have been used to study the influence of the choice of a solvent phase on the particle size and dispersion of the metal deposited on the BN support. The modifications undergone by the support during the deposition of palladium in different solvents have also been studied. Through the use of the same deposition procedure, different noble metal coatings (Pt, Pd, Au, and Ag) have been prepared. The acidic and redox characteristics of the resulting samples were characterized by temperature-programmed reduction and adsorption microcalorimetry. The catalytic performances of these materials were tested in the total oxidation of methane in lean conditions (excess oxygen and presence of water).

1. Introduction

Due to its remarkable properties, boron nitride has shown definite promise as a novel support in catalysis and as a replacement for traditional oxide supports in different processes. Boron nitride has not been studied extensively as a support; however, there are recent reports in the literature about the good performance of boron-nitride-based catalysts in some catalytic processes. Several recent studies describe the use of BN-supported noble metals for the deep oxidation of volatile organic compounds (VOCs). Wu et al.[1] have shown that a Pt/BN catalyst can remain active for 80 h at 185 °C, while the activity of traditional Pt/γ-Al_2O_3 at the same temperature was found to decrease continuously with time. Lin et al.[2] and Wu et al.[3] have studied Pt/BN as a catalyst for the deep oxidation of methanol and benzene. They concluded that Pt particles form weaker bonds with the BN surface, compared to γ-Al_2O_3. This weak bonding facilitated the reduction of the Pt particles. The reduced state of the Pt particles on Pt/BN caused a weaker oxygen bonding on the surface of Pt in the presence of oxygen, leading to a larger supply of reactive oxygen species and thus promoting the catalytic oxidation. Jacobsen[4] studied a Ba−Ru/BN catalyst for ammonia synthesis and found that the activity of this catalyst is significantly higher than that of traditional catalysts used in ammonia synthesis. The author concluded that the stable activity of the Ba−Ru/BN catalyst is related to the thermodynamic stability of BN under the test conditions. Boron nitride has also been used as support for vanadium oxide and showed promising results in propane oxidation.[5] Wu et al.[6] have also presented favorable findings for the selective hydrogenation of α,β-unsaturated aldehydes into unsaturated alcohols by employing BN-supported Pt−Sn catalysts.

Catalytic combustion of methane has drawn much attention in recent years because methane is a well-known greenhouse gas and the most stable and abundant alkane. Moreover, methane combustion is an attractive source of energy because of the large world reserves of CH_4 as natural gas and its low levels of sulfur- and nitrogen-containing impurities. The two main applications of methane combustion where catalysis may play a role are in gas turbines for generating power and in automobile exhausts for removing small amounts of methane from the emissions of methane-burning engines. In the first case, the catalyst is operating at temperatures of up to 800 °C, while in the latter case, the catalyst must exhibit activity below 300 °C.[7−9] Since both carbon dioxide and water are products of the combustion reaction, it is important that the effect of these compounds on the activity of the catalysts should be negligible. Although in

* Author to whom correspondence should be addressed. Fax: (33) 472 44 53 99. E-mail: aline.auroux@catalyse.cnrs.fr.
[†] Centre National de la Recherche Scientifique.
[‡] Università di Milano.
[§] Université de Pau.
[||] "Ilie Murgulescu" Institute of Physical Chemistry of the Romanian Academy.
[⊥] Université Claude Bernard Lyon 1.

10.1021/jp060183x CCC: $33.50
Published on Web 06/03/2006

the case of carbon dioxide there is no clear agreement as to its effect on methane combustion,[9] it is commonly agreed that water has a negative effect on the combustion reaction over traditional supported noble metal catalysts such as Pd/Al_2O_3.[9−11]

It is therefore necessary to develop novel materials that are able to withstand high temperatures and can serve as catalysts or supports for these reactions even in humid atmospheres.

In this work, the deposition of palladium on boron nitride supports has been carried out using protic or aprotic solvents as dispersing phases. The route using aprotic solvents involves the choice of palladium acetylacetonate as the precursor and anhydrous hydrazine as the reducer. The choice of BN as the support was also directed by the search for new hydrophobic supports with high thermal conductivity, adapted to high-energy oxidation reactions under severe conditions. Boron nitride is one of the most interesting non-oxide ceramic materials because of its low density, excellent resistance to chemical attacks, high melting point, good thermal conductivity, and high stability with respect to oxidation.[12−14] Contrary to BN, materials traditionally used as supports of active phases (oxides such as γ-Al_2O_3 and SiO_2) possess low thermal conductivity and many acidic and basic sites, causing sintering of the supported metal on hot spots and coverage of the catalyst by water.[15,16] Moreover, the metal−support interaction present in most oxide-supported metal catalysts has a negative influence on the catalytic activity.[15,17]

Concerning the metals deposed as active phases, previous works[13,18] have demonstrated that the particle size is an important parameter driving the catalytic properties; large particles with dimensions around 20 nm or aggregates have been shown to be inefficient. Noble metal nanoparticles are usually obtained by reducing a metal precursor with a strong reducer; this reaction is often performed using borohydrides in protic solvents.[19] However these chemicals are very strong reducers, and the particles obtained by this process have been shown to present a broad size dispersion. Moreover, the presence of borohydride hydrolysis residues such as sodium or potassium borates can have a negative impact on the purity of the catalyst. The reducing character of hydrazine is known to be softer than that of borohydrides, and the solubility of hydrazine is rather high in almost all solvents. For example, hydrated hydrazine has been used to prepare magnetic nanocomposites[20] from organometallic complex salts by ligand displacement and cation reduction to metal in a single operation.

Noble metals are extensively used as the active components in many industrial catalytic processes and for the conversion of environmentally unfriendly chemicals in gaseous emissions. Among noble metals, Pt and Pd are the most commonly used and studied catalysts.[21,22] Platinum and palladium are known to present low light-off temperatures in the oxidation of hydrocarbons and other organic chemicals.[22−24] The activity of palladium is generally better than that of platinum for the conversion of methane, but it is lower for the transformation of other chemicals.[24] Silver and gold have also been used with good results as active phases in hydrocarbon oxidation reactions.[25−27]

In this paper, the synthesis of palladium nanoparticles and their deposition on high-surface-area boron nitride have been performed using seven different dispersion phases. The sizes of the particles and their dispersion have been studied using X-ray diffraction (XRD) and transmission electron microscopy (TEM). The support and catalysts have been fully characterized to compare the roles played by the deposed metal in the catalytic performances of the studied samples. In the second part of this work, using the same support, BN, and the same deposition conditions, different metals have been considered, and platinum, gold, and silver metal particles have been deposed, leading to catalysts which were tested in the reaction of total oxidation of methane in severe conditions (excess of oxygen and presence of water). To our knowledge, no other groups have reported studies about the use of BN-supported catalysts for methane oxidation/combustion reactions.

2. Experimental Section

2.1. Materials. All the experiments were performed using as the catalyst support a boron nitride powder from Starck exhibiting a hexagonal nonisotropic structure formed of 5 μm platelets with 3 μm thickness (as determined by scanning electron microscopy (SEM)) and presenting a surface area of 136 $m^2\ g^{-1}$. The palladium precursor was palladium(II) acetylacetonate, provided by Aldrich and used as received. For the other noble metals the precursors used were hexachloroplatinic(IV) acid (Metalor), hydrogen tetrachloroaurate(III) (Strem), and silver nitrate (Strem) for Pt, Au, and Ag, respectively. The solvents or dispersing phases used were supplied by SDS Company for the organic compounds such as benzene, ethyleneglycol−dimethyl ether (monoglyme or glyme), tetrahydrofurane (THF), diethyleneglycol−dimethyl ether (diglyme), 2-propanol, and ethyleneglycol (glycol). They were all HPLC grade without stabilizer, anhydrous (water amount lower than 0.03 wt %), and kept on active 5 Å molecular sieves. Anhydrous hydrazine (water amount lower than 0.1 wt %) was prepared in the laboratory following a method described in the literature.[28]

2.2. Preparation of the Samples. In a typical preparation, 4 g of BN powder was added to 200 cm^3 of dispersing phase in a three-necked flask equipped with a refrigerant and under argon flow, under a vigorous stirring during 15 min. Approximately 0.1145 g of palladium(II) acetylacetonate (0.376 mmol leading to 40 mg of metallic palladium) were then added, while stirring for another 15 min to obtain the precursor dissolution and a homogeneous suspension of the support. A solution of 1 g of anhydrous hydrazine (31.25 mmol) dissolved into 100 cm^3 of solvent was then added drop by drop into the suspension for 10 min. The reaction occurred instantaneously, leading to a dark gray color due to the formation of metallic palladium. The stirring was maintained for 1 h and then stopped. After the catalyst was allowed to settle overnight, a clear liquid phase was easily separated from the solid. The catalyst was then dried under low pressure (10^{-2} h Pa during 10 h). Very thin powders were obtained, with a light gray color due to the metal deposed. The samples were labeled in relation to the dispersion liquid used: Pd/BN_bz when prepared in benzene, Pd/BN_gly for monoglyme, Pd/BN_wat for water, Pd/BN_thf for THF, Pd/BN_digl for diglyme, Pd/BN_isop for 2-propanol, and Pd/BN_glc for glycol. All samples were calcined up to 500 °C for 10 h under air flow, using a heating rate of 1 °C min^{-1}. The same preparation procedure was followed, using ethyleneglycol as solvent and the respective metal precursors, to obtain Pt/BN_glc, Ag/BN_glc, and Au/BN_glc catalysts.

2.3. Characterization. The physicochemical properties of the catalysts were determined using several techniques. The specific surface areas of the samples were measured by N_2 adsorption and calculated from the Brunauer−Emmett−Teller (BET) method. Prior to surface area determination, the samples were outgassed at 100 °C overnight and then at 400 °C for 6 h. The pore size distribution of each sample was determined from the desorption branch of the N_2 isotherm, using an ASAP 2010M apparatus, from Micromeritics, and gave evidence for some

microporosity in the parent BN. Therefore, deBoer's *t*-plot analysis was used to obtain the micropore surface area. For this support, approximately 36 $m^2\ g^{-1}$ of the surface area was contained in micropores (i.e., radius less than 1 nm), and 100 $m^2\ g^{-1}$ was in larger pores. A micropore volume of 0.0168 $cm^3\ g^{-1}$ was found by the *t*-method. Due to the presence of micropores, the BET method using nitrogen is perhaps not the most appropriate technique for determining the surface area of high-surface-area BN samples. However, to compare our results with those from the literature, we used this method. Some microporosity was also observed by Lindquist et al.[29] who reported a micropore surface area of 43 $m^2\ g^{-1}$ and surface area of larger pores of ~307 $m^2\ g^{-1}$ for a BN sample heated at 1500 °C for 24 h. Dibandjo et al.[30] reported a BN surface area of 540 $m^2\ g^{-1}$ using the BET method on their samples, and Han et al.[31] reported a surface area of 168 $m^2\ g^{-1}$ for a porous BN.

X-ray diffraction spectra were recorded using a Bruker (Siemens) D5005 apparatus. The concentrations of the supported metals were determined by chemical analysis using inductively coupled plasma atomic emission spectroscopy (ICP-AES). For that purpose, the samples were treated with a mixture of H_2SO_4 + HF + HNO_3 to dissolve them completely. The morphologies of the different samples have been examined using SEM, and the active phase dispersion and particle size have been measured by TEM. Scanning electron microscopy images were obtained from a JEOL 55 CF (CMEABG, UCB, Lyon), and TEM pictures were recorded using a JEOL 2010 (IRC, Lyon). The Pd particle sizes were calculated from the TEM micrographs obtained after calcination, taking into account about 20 particles out of the aggregates to obtain an average value for the dispersed active phase. X-ray photoelectron spectrometry (XPS) analysis was performed using a Surface Science Instruments 301 spectrophotometer with monochromatic Al Kα radiation to analyze the Pd dispersion and the possible formation of boron oxides. The 1s binding energy of boron was considered to survey the surface chemical species of the hexagonal boron nitride (h-BN) samples. Reference binding energies (BEs) were 190.5 eV for BN and between 192.2 and 193.0 V for BO_x.[1,2,12] Thermogravimetry experiments were performed in a TG-DSC 111 apparatus from Setaram, in air up to 600 °C using a heating rate of 5 °C min^{-1}. Infrared spectra were recorded with a Vector 22 spectrometer from Bruker with KBr windows, working in a spectral range of 4000−400 cm^{-1}. The pellets were a mixture of 100 mg of KBr, dried at 120 °C, and 7 mg of studied catalyst.

Microcalorimetric studies of ammonia adsorption were performed at 80 °C in a heat flow calorimeter (C80 from Setaram) linked to a conventional volumetric apparatus and equipped with a Barocel capacitance manometer for pressure measurements. The samples were pretreated in a quartz cell by heating overnight under vacuum at 400 °C with a heating rate of 0.6 °C min^{-1}. The differential heats of adsorption were measured as a function of coverage by repeatedly sending small doses of gaseous ammonia onto the catalysts until an equilibrium pressure of about 67 Pa was reached.[32] The samples were then outgassed for 30 min at the same temperature, and a second adsorption was performed at 80 °C on each sample until an equilibrium pressure of about 27 Pa was attained, to calculate the amount of irreversibly chemisorbed ammonia at this pressure, which provides an estimate of the number of strong acidic sites.

Temperature-programmed reduction (TPR) was performed in a custom-made apparatus already described in the literature,[33] equipped with a U-shaped quartz tube microreactor and surrounded by a furnace controlled by a programmed heating system. Prior to each test, a sample of about 150 mg of catalyst was pretreated in an argon flow at a rate of 20 $cm^3\ min^{-1}$ at 400 °C (2 °C min^{-1}). A reducing gas mixture composed of 5% H_2 plus 95% Ar was employed for the reduction, at a flow rate of 20 $cm^3\ min^{-1}$ and with a heating rate of 10 °C min^{-1} from room temperature to 600 °C. The hydrogen consumption was detected with a thermal conductivity detector (TCD).

TABLE 1: Changes in Surface Area of the BN Support after Swelling in a Solvent

sample	S_{BET} ($m^2\ g^{-1}$)	mass loss H_2O (wt %)
BN fresh	136	2
BN calcined	136	1.7
BN_gly calcined	233	1.3
BN_isop calcined	292	5.1

2.4. Catalytic Tests. Catalytic tests of the methane oxidation reaction were performed in a quartz tubular microreactor. The samples were prepared by adding 0.05 g of catalyst to 1 g of quartz (1:20 dilution). The powders tested and the quartz used for dilution were ground and sieved separately to obtain particles of 0.2−0.3 mm. The samples were pretreated for 4 h at 400 °C in O_2/He (20% v/v) flow. A set of mass flow controllers (Bronkhorst, Hi-Tec) made it possible to determine accurately the composition of the reactant mixture: 1500 ppm CH_4 and 30 000 ppm O_2 in helium. The reaction was performed under wet atmosphere by passing the reactant mixture through water. A catalytic test was also performed on the sample Pd/BN_glc using a dry gas mixture to compare the behavior of the catalyst in the presence of dry and water-saturated reactant gases. The reaction was carried out at fixed space velocity (gas hourly space velocity = 42 000 h^{-1}) and variable temperature. Seven different temperatures in the interval of 400−700 °C were chosen, each temperature being held for 90 min. The reactant and exit gas streams of the reactor flowed through a gas cell (path length 2.4 m multiple reflection gas cell) in the beam of a Fourier transform infrared (FTIR) spectrometer (Bio-Rad with -DTGS detector). The spectrometer response permitted quantitative analyses for CH_4 (1360 cm^{-1}), CO (2086 cm^{-1}), and CO_2 (721 cm^{-1}). The conversion percentages and selectivities were calculated from the measured concentrations of the reactants and products.

3. Results and Discussion

3.1. Behavior of the BN Support during the Chemical Treatment. To verify the inertness of the BN support during the metal deposition, samples of BN powder were dispersed in the employed solvents, added with hydrazine, and then separated and calcined as in the experimental procedure for the preparation of the catalysts. From this procedure, the diffraction patterns did not show any difference in the widths of the BN diffraction lines, and the IR spectra did not reveal any hydrolysis. The surface area was the only parameter that changed upon such chemical treatment. The BET surface area and water loss (as determined by TGA) of the support after chemical treatment and calcination are given in Table 1. These changes in surface area can be explained by an increase of microporosity originating from specificities of the BN structure. The hexagonal BN crystallographic structure consists of three BN groups stacked into a hexagonal framework, leading to BN layers, similar to graphite. These layers are bound together through anisotropic bonds leading to a very oriented compound. It seems that when BN powders are swelled in a solvent an important fraction of the solvent molecules enter inside the BN layers and open nanopores during the calcination process. The increase in surface area can therefore be ascribed to the opening of nanopores by

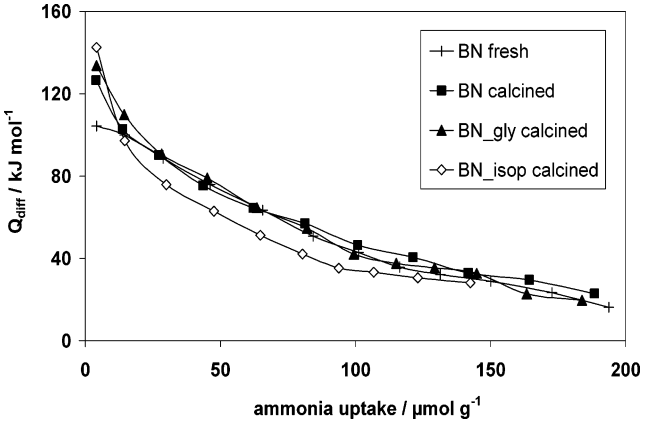

Figure 1. Acidity of the support; differential heats of ammonia adsorption vs coverage.

TABLE 2: Calorimetric Data for NH_3 Adsorption at 80 °C on BN Supports

		ammonia uptake		
sample	solvent	n_{total}[a] (μmol g^{-1})	n_{reads}[b] (μmol g^{-1})	n_{irr}[c] (μmol g^{-1})
BN fresh		141	63	78
BN calcined		145	66	79
BN_gly calcined	glyme	139	66	73
BN_isop calcined	2-propanol	110	56	54

[a] Amount of NH_3 absorbed under an equilibrium pressure of 27 Pa. [b] Amount of NH_3 reabsorbed after pumping at 80 °C under an equilibrium pressure of 27 Pa. [c] Amount of irreversibly chemisorbed ammonia.

the solvent trapped during the chemical treatment, which then evolved during the calcination, while the crystallographic parameters remain unchanged. Scanning electron microscopy micrographs reveal that the layer structure of boron nitride is changed only at the edge of the BN platelets, as the BN structure in the platelets is very slightly affected by the edge effects of the splitting. The weight loss measured on calcined samples corresponds to the water uptake when the catalyst is kept without any special care. The dispersing phases did not influence noticeably the acidity of the BN supports (Figure 1). The initial heat of adsorption of ammonia on the parent BN support was measured to be 105 kJ mol^{-1}; this is indicative of a relatively weak acidity, compared to an oxide support such as γ-Al_2O_3. Calcined BN and BN_gly samples display differential heat curves similar to the fresh support, except for the initial heats which are higher than 120 kJ mol^{-1}. Meanwhile, the shape of the curve of heat of interaction versus coverage for ammonia adsorption over the BN_isop calcined powder is also similar to the previous ones but shifted toward lower heats, except for the initial heat value. A slightly lower number of acid sites were titrated (Table 2), which is consistent with an increase of the nanoporosity of the support.

3.2. Pd Catalysts Obtained using Various Dispersing Phases. Several dispersing phases, protic or aprotic and with different physical and chemical properties, were used to dissolve the precursor, with the aim to avoid clustering of the nanoparticles produced. A sample diffraction pattern is given in Figure 2, which represents the XRD spectra of uncalcined Pd/BN_thf and the corresponding fresh support. These diffraction patterns show that the BN support was not modified by the chemical treatment, and no hydrolysis occurred during the palladium deposition. Palladium is clearly characterized by its (111) diffraction peak at $2\theta = 39.95°$ with a small difference from the 40.2° theoretical value. This increase of the lattice parameter

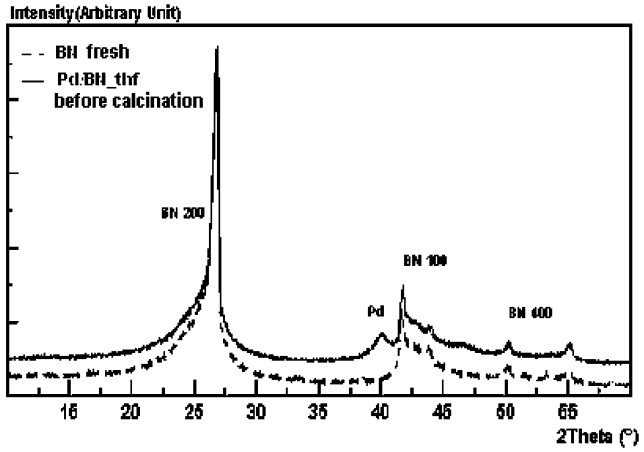

Figure 2. X-ray diffraction patterns of the Pd/BN_thf catalyst and the corresponding BN support.

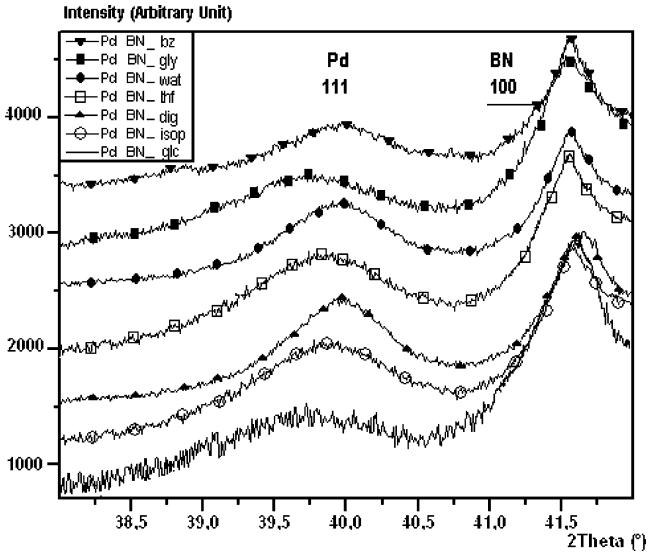

Figure 3. X-ray diffraction patterns of the Pd deposed on BN using different solvents before calcination.

could be related to the presence of a small amount of oxide or oxygen in the metal. Figure 3 represents the Pd(111) diffraction line for all uncalcined samples as synthesized in different solvents. The only difference between the various spectra is in the width of the (111) diffraction line of metallic palladium.

The size of the palladium particles can be calculated from the X-ray diffraction pattern recorded using the Scherrer formula[34] applied to the full width at half maximum of the (111) Pd diffraction line

$$(L = K\lambda/B_{struct} \cos \theta)$$

In this formula, K describes the crystalline shape factor of the particles (here K is 0.85 as proposed for cubic systems), λ is the wavelength, and θ is the incidence angle. The term B_{struct} describes the structural broadening, which is the difference in the integral profile between a standard reference (0.05° measured for silicon reference with the same intensity) and the sample to be analyzed. Table 3 gathers the measured values after standardization of the spectra using the (100) BN diffraction line intensity as an internal reference.

Important changes appeared after calcination of the freshly prepared samples. The heating in air induced an oxidation of palladium into the oxide, PdO, which led to an increase of the particle size. The measured increases were more important than

TABLE 3: Characterization of the Catalysts

sample	solvent	S_{BET} ($m^2\ g^{-1}$)	$V_{micropore}$[a] $cm^3\ g^{-1}$	total pore volume[b] ($cm^3\ g^{-1}$)	average pore diameter[c] (nm)	XPS[d] BN (%)	XPS[d] BO_x (%)	Pd amount XPS (at. %)	Pd amount ICP (wt %)	Pd particle size (nm) XRD[e]	Pd particle size (nm) XRD[f]	Pd particle size (nm) TEM[g]
BN fresh		136	0.0168	0.0966	4.7	100	0					
Pd/BN_bz	benzene	73	0.0034	0.0892	7.4	85	15	0.1	0.94	7	16	12
Pd/BN_gly	glyme	179	0.0215	0.1128	4.4	96	4	0.6	0.89	7	15	14
Pd/BN_wat	water	254	0.0504	0.1382	4.0	100	0	0.4	0.95	11	18	16
Pd/BN_thf	THF	138	nd	nd	nd	93	7	0.5	0.94	9	12	15
Pd/BN_digl	diglyme	215	nd	nd	nd	100	0	0.4	0.99	13	15	nd
Pd/BN_isop	2-propanol	229	nd	nd	nd	100	0	0.5	0.94	9	14	15
Pd/BN_glc	ethyleneglycol	221	nd	nd	nd	93	7	0.6	0.74	7	16	nd

[a] Micropore volumes obtained by the *t*-method. [b] Total pore volume at $P/P_0 = 0.98$. [c] Average pore diameter according to the BJH method (adsorption branch). [d] Relative concentrations of boron compounds (BN and BO_x). [e] Size of the palladium particles calculated from X-ray diffraction patterns before calcination. [f] Size of the palladium particles calculated from X-ray diffraction patterns after calcination. [g] Size of the palladium particles calculated from TEM micrographs after calcination.

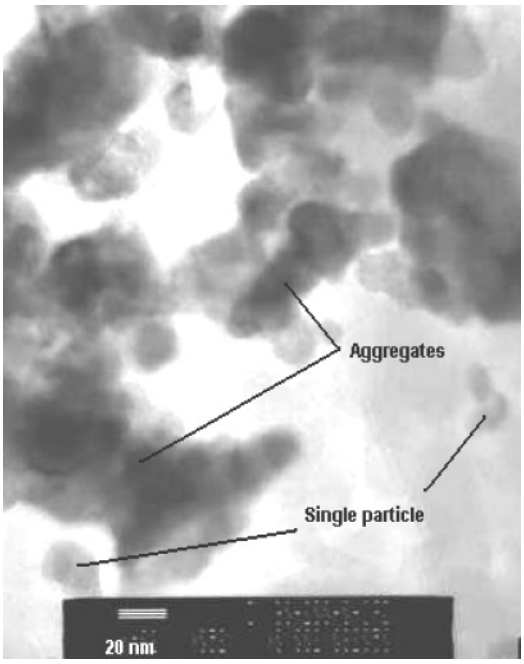

Figure 4. Transmission electron microscopy images of the Pd/BN_gly sample after calcination under air flow.

expected and were found to be irreversible, after reduction of PdO in a flow of 5% H_2/Ar. The size of the particles remained unchanged after the oxidation−reduction cycle.

The TEM micrograph presented in Figure 4 shows clearly that particles are stacked into larger clusters; this clustering occurred during the palladium oxidation−reduction cycle. It is well-known that palladium oxidation was found to be dependent on the dispersion; the lower the dispersion, the lower the Pd oxidation extent. Moreover, the rate of the oxidation is strongly dependent on temperature.[21,35,36] In our case, the nanoparticles are gathered at the support grain border, and they aggregate after heating and oxidation of palladium, leading to larger particles. The small size particles (about 7 nm) observed initially aggregated into particles of sizes of about 15 nm, whereas larger particles were less affected. With the same metal amount the larger particles were less numerous than the small ones, as observed on the TEM micrograph. The average particle size was enhanced by the sintering, as shown by Table 3, where the values obtained from XRD and TEM are consistent. In addition, Table 3 gives the amounts of Pd, determined either by ICP (wt %) or XPS (at. %) methods. We found that the binding energies of Pd $3d_{5/2}$ vary between 337.5 and 338.4 eV, which can be assigned to the presence of Pd(II). X-ray photoelectron spectroscopy results show also that the worst dispersion of Pd is achieved in benzene solvent. Moreover, the relative concentrations of boron species at the surface were also determined by XPS. We observed a slight oxidation of the surface of some samples; the Pd/BN_bz sample expressed the highest relative concentration of BO_x. As can be seen in Table 3, all samples present surface areas higher than that of the parent support, except for the Pd/BN_bz catalyst. While the increase in S_{BET} can be related to the BN structure as suggested in subsection 3.1, the decrease in surface area observed for Pd/BN_bz could be assigned to the poor solubility of hydrazine in benzene (see the preparation method), which induced a polyphasic reaction favoring a partial hydrolysis leading to the formation of oxide derivatives. Accordingly, as mentioned above, XPS measurements revealed the presence of B_2O_3 (relative concentration 15%) in this sample. In addition, FTIR spectra (Figure 5) confirmed the partial hydrolysis and the presence of hydroxyl groups. All the samples except Pd/BN_bz presented FTIR spectra similar to the BN support. For this reason, only one sample spectrum, Pd/BN_digl, was represented in Figure 5 together with BN and Pd/BN_bz.

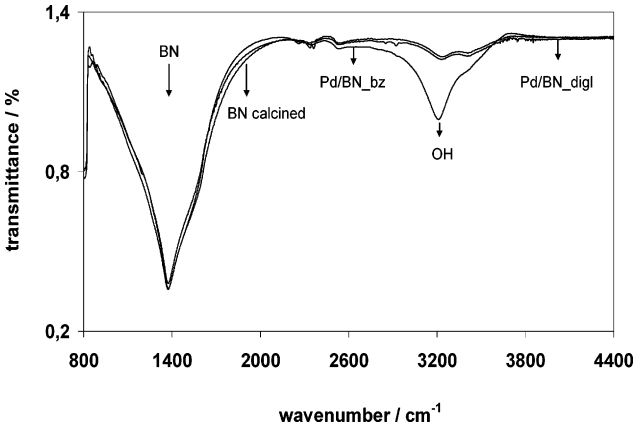

Figure 5. Fourier transform infrared spectra of the calcined BN support, Pd/BN_digl, and Pd/BN_bz.

DeBoer's *t*-plot analysis was used to obtain the micropore surface area. For samples Pd/BN_bz, Pd/BN_gly, and Pd/BN_wat, the micropore surface areas were 8, 47, and 109 $m^2\ g^{-1}$, respectively, which explains the changes in surface areas observed by the BET method for these samples compared to BN fresh support (Table 3). Table 3 displays also the micropore volume, the total pore volume, and average pore diameter. The pore size diameters were obtained from the adsorption branch of the isotherm using the corrected form of the Kelvin equation by means of the Barrett−Joyner−Halenda (BJH) method.

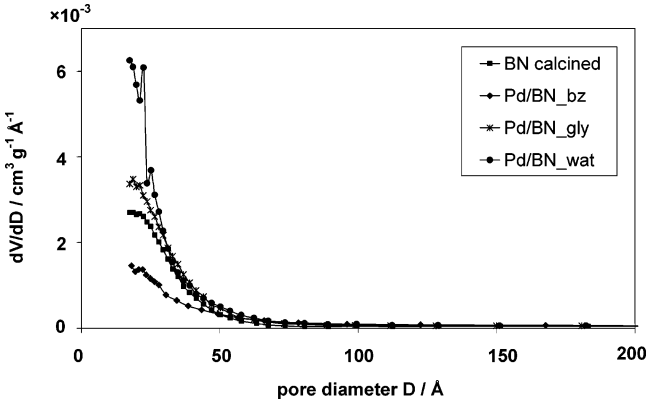

Figure 6. Derivative of the pore volume as a function of the pore diameter for some Pd/BN samples.

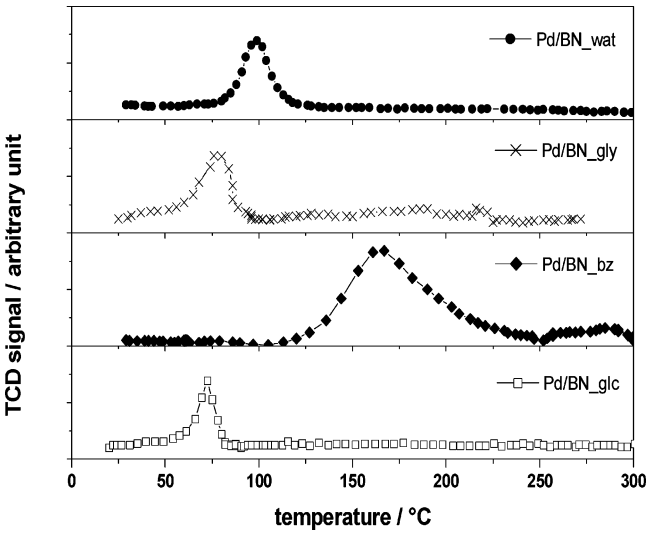

Figure 7. Thermoprogrammed reduction profiles of Pd/BN samples under H_2/Ar flow.

TABLE 4: Temperature-Programmed Reduction Results Obtained for the Catalysts Studied Using 5% H_2 + Ar

sample	Pd reduced (%)	T_M (°C)
Pd/BN_bz	35	160
Pd/BN_gly	23	76
Pd/BN_wat	19	99
Pd/BN_glc	23	72

Figure 6 displays the derivative of the pore volume as a function of pore diameter, for some of the samples studied. In comparison to the BN support, the microporosity was increased for all samples except for Pd/BN_bz, confirming the above results and the pore blocking by some boron oxide. The micropore volume measured by the *t*-method is consistent with the surface area determination; the sample prepared using benzene, which is the most oxidized, presents the smallest surface area and also the smallest pore volume (Table 3).

Temperature-programmed reduction (TPR) experiments were also performed on some of the samples presenting the most different surface areas (Pd/BN_bz, Pd/BN_gly, Pd/BN_wat, and Pd/BN_glc). The H_2 TPR profiles of Pd/BN catalysts recorded up to 300 °C are shown in Figure 7. No hydrogen uptake peaks were observed at higher temperatures. For all the tested samples, the H_2 TPR profiles show only one peak of reduction, with a maximum below 100 °C, except Pd/BN_bz which displayed a maximum at 160 °C (Table 4). The reduction temperature for Pd/BN_bz is higher than those for the other samples and could be related to the presence on the support of boron oxide, which can react partially with palladium oxide to form a more stable compound.

Stoichiometrically, the theoretical H_2 consumption for the reduction of PdO to Pd should be 88 μmol g^{-1} for Pd/BN_bz, 84 μmol g^{-1} for Pd/BN_gly, 89 μmol g^{-1} for Pd/BN_wat, and 70 μmol g^{-1} for Pd/BN_glc, respectively. The hydrogen uptake, calculated from the area under the experimental curve, is 31 μmol g^{-1} for Pd/BN_bz, 19 μmol g^{-1} for Pd/BN_gly, 17 μmol g^{-1} for Pd/BN_wat, and 16 μmol g^{-1} for Pd/BN_glc, respectively. The degree of PdO reduction for each catalyst is listed in Table 4, confirming the results obtained by TEM: The palladium nanoparticles deposed on the support surface had a slight tendency to form stacked aggregates during the thermal oxidation−reduction cycles.

TABLE 5: Calorimetric Data for NH_3 Adsorption at 80 °C on the BN-Supported Pd Catalysts

		ammonia uptake		
sample	solvent	n_{total}[a] (μmol g^{-1})	n_{reads}[b] (μmol g^{-1})	n_{irr}[c] (μmol g^{-1})
Pd/BN_bz	benzene	198	42	156
Pd/BN_gly	glyme	183	69	114
Pd/BN_wat	water	195	92	103
Pd/BN_thf	THF	193	68	125
Pd/BN_digl	diglyme	172	73	99
Pd/BN_isop	2-propanol	160	74	86
Pd/BN_glc	glycol	179	49	130

[a] Amount of NH_3 absorbed under an equilibrium pressure of 27 Pa. [b] Amount of NH_3 reabsorbed after pumping at 80 °C under an equilibrium pressure of 27 Pa. [c] Amount of irreversibly chemisorbed ammonia.

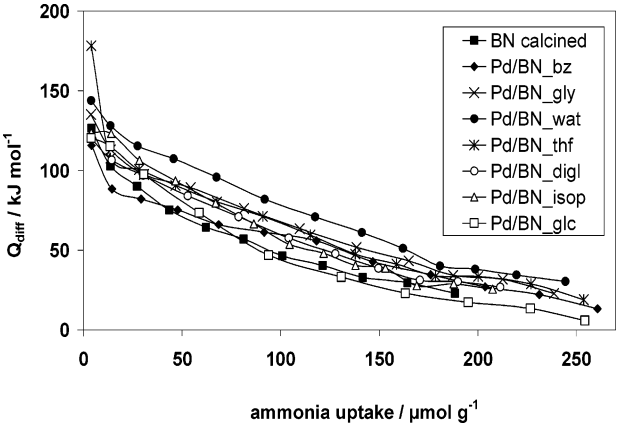

Figure 8. Differential heats of ammonia adsorption vs coverage for calcined BN support and Pd/BN catalysts prepared in different solvents.

The acidic character of the catalysts was estimated by ammonia adsorption microcalorimetry. It is well-known that besides determining quantitatively the surface acidity of solids (the acidity playing an important role in all catalytic processes) adsorption microcalorimetry allows the determination of the strength distribution of the sites. The results obtained are presented in Table 5 and Figure 8. The initial values of the differential heats of ammonia adsorption indicate the existence of stronger acid sites on Pd/BN_gly, Pd/BN_wat, and Pd/BN_thf in comparison with the calcined BN support. The influence of the preparation method on the acid strength distribution of the catalysts and consequently on the surface state modification of the BN support in the dispersing phase is evident.

The catalytic performances of samples were tested in methane oxidation. Table 6 presents the CH_4 conversions calculated from the residual methane concentration at each reaction temperature. The first test on Pd/BN_glc was performed using a dry mixture

TABLE 6: Methane Conversion Using Different BN-Supported Pd Catalysts

	CH_4 conversion (%)				
		wet conditions			
T (°C)	dry conditions Pd/BN_glc	Pd/BN_gly	Pd/BN_glc	Pd/BN_wat	BN calcined
400	0	0.1	0.2	0.6	0
500	1.8	0.2	0.8	0.9	0
550	3.5	0.7	1.3	4.1	0
600	5.3	14.6	16.7	29.8	0
625	nd	38.8	36.4	64.1	1.3
650	nd	86.3	74.1	98.0	9.4
700	71.9	99.6	99.9	100.0	99.3

of reactant gases. The results obtained show a low methane conversion (around 70% conversion at 700 °C). After the catalyst was cooled to room temperature and 2 h rest under dry reactive gas atmosphere, a second run was performed on the same sample using a water-saturated gas mixture. The enhancement of the conversion at 700 °C was important (around 90% methane conversion), which led us to evaluate the conversion capabilities of the other catalysts only under wet conditions.

The BN support was totally inactive below 625 °C. However, a slight conversion of about 9% was observed at 650 °C; at this temperature, only CO and H_2O were obtained as products. The methane conversion increased significantly at 700 °C, with CO_2 formation; however, CO remained present in important amounts, probably due to homogeneous reactions.

The palladium catalysts supported on boron nitride showed roughly similar activities, as can be seen in Figure 9. The Pd/BN catalysts were inactive in methane oxidation at temperatures lower than 400 °C. At temperatures ranging between 400 and 650 °C, important concentrations of CO were detected in the products stream. The main oxidation products became CO_2 and H_2O only above 650 °C, as can be seen for example in Figures 10 and 11 where CO and CO_2 productions are plotted versus temperature. The onset temperatures ($X_{CH_4} = 15\%$) decreased in the order BN > Pd/BN_gly > Pd/BN_glc > Pd/BN_wat, which can be related to the calculated activation energies (238 kJ mol^{-1} for Pd/BN_gly, 200 kJ mol^{-1} for Pd/BN_glc, and 160 kJ mol^{-1} for Pd/BN_wat).

Across the entire temperature range, Pd/BN catalysts present higher conversions than boron nitride alone. Similarities between the activities at 700 °C suggest that homogeneous gas-phase reactions could be also involved in methane oxidation at this temperature. Above 625 °C, we conjecture that the high amount of CO formed is mainly due to the support, while the main role of the palladium deposed as the active phase is to improve the

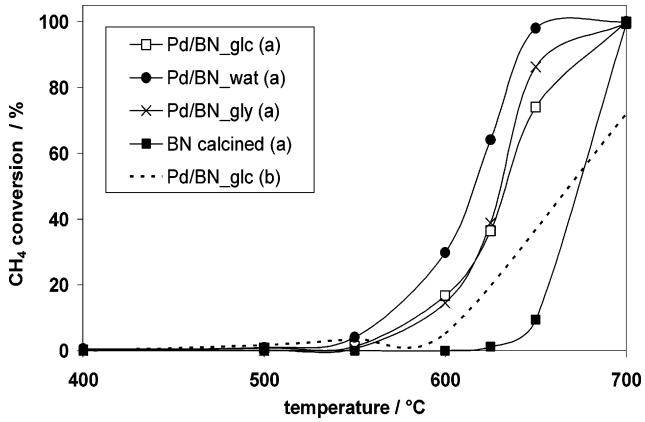

Figure 9. Activity for methane oxidation over boron-nitride-supported palladium catalysts: (a) in the presence of water, (b) in dry conditions

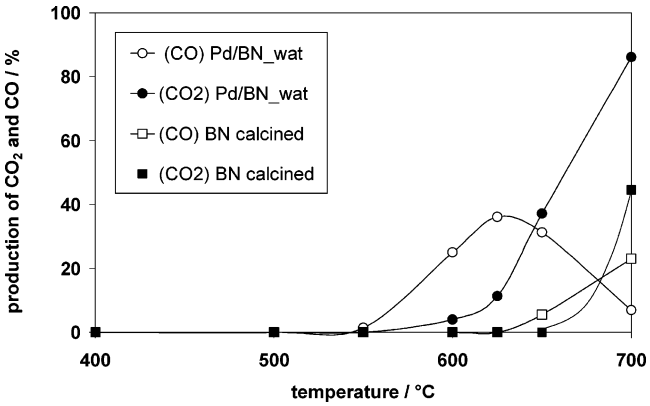

Figure 10. Comparison of the productions of CO and CO_2 during CH_4 oxidation for the Pd/BN_wat catalyst and the BN support

complete oxidation and to shift the onset of oxidation toward a lower temperature.

Concerning the use of BN as a support for noble metals in the CH_4 combustion reaction, we observed light-off temperatures ($X_{CH_4} = 50\%$) higher than those reported in the literature for the traditional catalysts (Pd/Al_2O_3 and Pd/ZrO_2).[1,23,37−41] However, we have to point out that our experiments were carried out under very severe conditions with a O_2/CH_4 ratio equal to 20 and in the presence of water. We observed a very good stability with time for Pd/BN catalysts, while the activity of Pd/Al_2O_3 catalysts under similar conditions decreased steadily over the first 20 hours.[14]

3.3. Supported Noble Metal (Pd, Pt, Ag, and Au) Catalysts. The above study of the performance of catalysts using palladium as the active phase on boron nitride supports has been completed by a comparison between different noble metals deposed using essentially the same preparation conditions (same BN support, dispersing phase and reducing agent). The efficiency of the catalysts obtained by deposition of small percentages of noble metals on the support is related to the size of the particles deposed and to the aggregation of the metal grains in larger clusters. Ethylene glycol was used as the dispersing phase, and the reduction of the precursors into metal was performed using hydrazine as described previously. However, the precursors used were not only acetylacetonates but also chlorinated derivatives. The use of inorganic precursors has induced important and unexpected differences in terms of amounts deposed and dispersion, related to the low solubility of halogenated compounds. The physicochemical characteristics of the catalysts obtained by the deposition of noble metals Pd, Pt, Ag, and Au on a BN support are presented in Table 7.

The metal particle sizes for each calcined sample were obtained from XRD data, using the Scherrer formula as described previously. In fact, after calcination of the catalyst in air, palladium was oxidized into PdO, as shown by the diffraction line at $2\theta = 38.84°$. For the Au catalyst, the amount of gold was clearly lower than expected, which can be explained by the low solubility and the differences in reactivity of the precursor employed.

The catalysts were tested in the reaction of methane oxidation under the same conditions as described for Pd/BN samples. The results are presented in Table 8. The light-off temperatures (50% methane conversion) increased from Ag/BN_glc (597 °C) to Au/BN_glc (613 °C) to Pt/BN_glc (614 °C) to Pd/BN_glc (634 °C) to BN (672 °C); the same trend is followed by the onset temperatures, which are 20−30 °C lower than the light-off temperatures. The main products of methane oxidation using boron-nitride-supported noble metal catalysts were CO and CO_2.

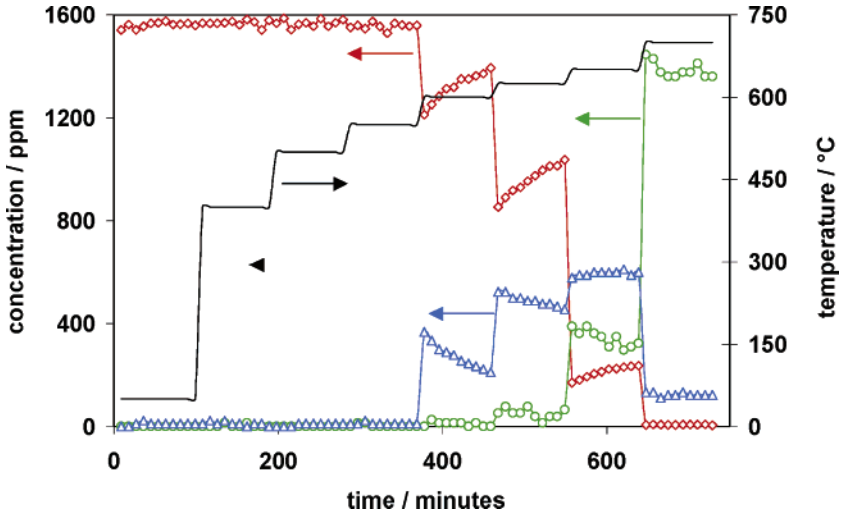

Figure 11. Concentrations of CH_4 (red), CO (blue), and CO_2 (green) vs time on stream during CH_4 oxidation over Pd/BN_gly.

TABLE 7: Physicochemical Properties of M/BN Catalysts, with M = Pd, Pt, Ag, Au

catalyst	S_{BET} (m^2 g^{-1})	metal (wt %)	metal particle size (nm)
Pd/BN_glc	221	0.74	16
Pt/BN_glc	220	0.73	12
Ag/BN_glc	250	1.16	31
Au/BN_glc	249	0.34	16

TABLE 8: Methane Conversion and the Ratio between CO and CO_2 Formation on Different M/BN Catalysts (Wet Conditions)

T (°C)	400	500	550	600	625	650	700
			CH_4 Conversion (%)				
Pd/BN_glc	0.2	0.8	1.3	16.7	36.4	74.1	99.9
Pt/BN_glc	0.3	0.6	3.6	30.1	66.7	97.9	100.0
Ag/BN_glc	0	0	4.0	53.0	89.0	99.2	99.8
Au/BN_glc	0.3	0.3	1.6	29.1	68.8	98.4	99.9
BN calcined	0	0	0	0	1.3	9.4	99.3
			CO/CO_2				
Pd/BN_glc	0	0	0	16.3	12.6	3.2	0.1
Pt/BN_glc	0	0	0.7	4.6	2.5	0.6	0.1
Ag/BN_glc	0	0	3.5	7.0	1.8	0.5	0.1
Au/BN_glc	0	0	0	35.3	3.7	0.8	0.1
BN calcined	0	0	0	0	0	5.6	0.5

At low temperatures the most abundant reaction product obtained was CO for all the catalysts studied, with Pt/BN_glc presenting the best selectivity for CO_2 above 550 °C. The selectivity toward CO was decreased by the addition of noble metals as active phases. The CO/CO_2 ratios measured over BN and BN-supported metal catalysts during methane oxidation are reported in Table 8. It can easily be seen that if the methane conversions on the Pt/BN_glc and Au/BN_glc catalysts at 600 °C are similar (Table 8), then the production of CO_2 is more pronounced when the active phase is platinum.

Surprisingly, the silver-based catalyst exhibited the highest performance despite a larger particle size. However this could be explained by the larger amount of silver deposed on the support; rescaling the conversion values for the same amount of noble metal led to a conversion at 600 °C of 46% for Ag, 41% for Pt, and 85% for Au respectively, which is more consistent with the published results.[21]

4. Conclusions

Boron nitride can be considered as a good candidate support for the preparation of high-performance catalysts, especially for use under severe conditions (high temperature, humid atmosphere). Several catalysts were prepared from commercial BN of about 130 m^2 g^{-1} of surface area on which a low percentage of noble metal was deposed. The surface area of the support was significantly enhanced (about 250 m^2 g^{-1}) by the chemical treatment, which led to the metal deposition, in most cases without hydrolysis or oxidation. The enhancement is due to the edge effect on the platelets, creating nanoporosity and a higher surface area. To test the conditions of deposition of the noble metal and the efficiency of the resulting catalysts, several preparation procedures have been applied, leading to significant differences in the metal particle sizes. Through the use of palladium as the reference metal and acetylacetonate as the precursor reduced by hydrazine, the various dispersing media tested have led to important differences in the particle size, from 7 to 13 nm, and the best results have been obtained using ethylene glycol as the dispersing phase. Unfortunately the palladium nanoparticles deposed on the support seemed to gather and even collapse into larger aggregates during the thermal oxidation−reduction cycles that were applied to the samples.

Through the use of the same support and the same deposition conditions, major differences were observed when different noble metals were used, illustrating the complexity of the rules that govern metal deposition from precursors and dispersing phases. Silver and gold seem to yield the most promising results.

Catalytic tests of methane oxidation performed under severe conditions have shown a good stability of the catalysts and a higher activity in the presence of water than that in dry atmosphere but excessively high conversion temperatures.

Acknowledgment. The authors thank W. Desquesnes and co-workers for isotherm measurements and M. Aouine for TEM pictures. G.P. thanks the ECO-NET project of the French Government for financial support.

References and Notes

(1) Wu, J. C. S.; Lin, Z. A.; Pan, J. W.; Rei, M. H. *Appl. Catal., A* **2001**, *219*, 117.
(2) Lin, C. A.; Wu, J. C. S.; Pan, J. W.; Yeh, C. T. *J. Catal.* **2002**, *210*, 39.
(3) Wu, J. C. S.; Fan, Y. C.; Lin, C. A. *Ind. Eng. Chem. Res.* **2003**, *42*, 3225.
(4) Jacobsen, C. J. H. *J. Catal.* **2001**, *200*, 1.
(5) Taylor, S. H.; Pollard, A. J. J. *Catal. Today* **2003**, *81*, 179.
(6) Wu, J. C. S.; Chen, W. C. *Appl. Catal., A* **2005**, *289*, 179.
(7) Lee, J. H.; Trimm, D. L. *Fuel Process. Technol.* **1995**, *42*, 339.
(8) Su, S. C.; Carstens, J. N.; Bell, A. T. *J. Catal.* **1998**, *176*, 125.

(9) Burch, R.; Urbano, F. J.; Loader, P. K. *Appl. Catal., A* **1995**, *123*, 173.
(10) Ribeiro, C. F.; Chow, M.; Dalla-Betta, R. A. *J. Catal.* **1994**, *146*, 537.
(11) Cullis, C. F.; Willatt, B. M. *J. Catal.* **1984**, *86*, 187.
(12) Postole, G.; Caldararu, M.; Ionescu, N. I.; Bonnetot, B.; Auroux, A.; Guimon, C. *Thermochim. Acta* **2005**, *434*, 150.
(13) Perdigón-Melón, J. A.; Auroux, A.; Guil, J. M.; Bonnetot, B. *Stud. Surf. Sci. Catal.* **2002**, *143*, 227.
(14) Postole, G.; Gervasini, A.; Auroux, A.; Bonnetot, B. *Chem. Eng. Trans.* **2004**, *4*, 271.
(15) Yao, H. C.; Sieg, M.; Plummer, H. K., Jr. *J. Catal.* **1979**, *59*, 365.
(16) Epling, W. S.; Hoflund, G. B. *J. Catal.* **1999**, *185*, 5.
(17) Carstens, J. N.; Su, S. C.; Bell, A. T. *J. Catal.* **1998**, *176*, 136.
(18) Perdigón-Melón, J. A.; Auroux, A.; Bonnetot, B. *J. Therm. Anal. Calorim.* **2003**, *72*, 443.
(19) Fiévet, F. Polyol Process. In *Fine Particles, Synthesis, Characterization and Mechanisms of Growth*; Sugimoto, T., Ed.; Marcel Dekker: New York, 2000; p 460.
(20) Yang, C.; Xing, J.; Guan, Y.; Liu, J.; Liu, H. *J. Alloys Compd.* **2004**, *385*, 283.
(21) Gelin, P.; Primet, M. *Appl. Catal., B* **2002**, *39*, 1.
(22) Zwinkels, M. F. M.; Järås, S. G.; Menon, P. G.; Griffin, T. A. *Catal. Rev.−Sci. Eng.* **1993**, *35* (3), 319.
(23) Choudhary, T. V.; Banerjee, S.; Choudhary, V. R. *Appl. Catal., A* **2002**, *234*, 1.
(24) Centi, G. *J. Mol. Catal. A: Chem.* **2001**, *173*, 287.
(25) Haruta, M. *Catal. Today* **1997**, *36*, 153.
(26) Kundakovic, Lj.; Flytzani-Stephanopoulos, M. *J. Catal.* **1998**, *179*, 203.
(27) Iglesias-Juez, A.; Fernández-Garcia, M.; Martinez-Arias, A.; Schay, Z.; Koppány, Zs.; Hungria, A. B.; Fuerte, A.; Anderson, J. A.; Conesa, J. C.; Soria, J. *Top. Catal.* **2004**, *30/31*, 65.
(28) Delalu, H.; Saïd, J.; Cohen-Adad, R. *J. Chim. Phys. Phys. Chim. Biol.* **1980**, *77*, 277.
(29) Lindquist, D. A.; Borek, T.; Kramer, S.; Narula, C.; Johnstone, G.; Schaeffer, R.; Smith, D.; Paine, R. T. *J. Am. Ceram. Soc.* **1990** *73*, 757.
(30) Dibandjo, P.; Bois, L.; Chassagneux, F.; Cornu, D.; Létoffé, J. M.; Toury, B.; Babonneau, F.; Miele, P. *Adv. Mater.* **2005** *17*, 571.
(31) Han, Wei-Qiang; Brutchey, R.; Tilley, T. D.; Zettl, A. *Nano Lett.* **2004**, *4*, 173.
(32) Auroux, A. *Top. Catal.* **1997**, *4*, 71.
(33) Jouguet, B.; Gervasini, A.; Auroux, A. *Chem. Eng. Technol.* **1995**, *18*, 243.
(34) Patterson, A. L. *Phys. Rev.* **1939**, *56*, 978.
(35) Datye, A. K.; Bravo, J.; Nelson, T. R.; Atanasova, P.; Lyubovsky, M.; Pfefferle, M. *Appl. Catal., A* **2000**, *198*, 179.
(36) Lieske, H.; Lietz, G.; Hanke, W.; Voelter, J. *Z. Anorg. Allg. Chem.* **1985**, *527*, 135.
(37) Yang, S.; Maroto-Valiente, A.; Benito-Gonzales, M.; Rodriguez-Ramos, I.; Guerrero-Ruiz, A. *Appl. Catal., B* **2000**, *28*, 223.
(38) Zwinkels, M. F. M.; Jaras, S. G.; Menon, P. G. *Catal. Rev.−Sci. Eng.* **1993**, *35*, 319.
(39) Oh, S. H.; Mitchell, P. J.; Siewert, R. M. *J. Catal.* **1991**, *132*, 287.
(40) Muto, K. I.; Katada, N.; Niwa, M. *Appl. Catal., A* **1996**, *134*, 203.
(41) Lyubovsky, M.; Pfefferle, L. *Appl. Catal., A* **1998**, *173*, 107.